

Hierarchical Distribution Matching for Probabilistically Shaped Coded Modulation

Tsuyoshi Yoshida, *Member, IEEE*, Magnus Karlsson, *Fellow, OSA; Senior Member, IEEE*,
and Erik Agrell, *Fellow, IEEE*

Abstract—The implementation difficulties of combining distribution matching (DM) and dematching (invDM) for probabilistic shaping (PS) with soft-decision forward error correction (FEC) coding can be relaxed by reverse concatenation, for which the FEC coding and decoding lies inside the shaping algorithms. PS can seemingly achieve performance close to the Shannon limit, although there are practical implementation challenges that need to be carefully addressed. We propose a hierarchical DM (HiDM) scheme, having fully parallelized input/output interfaces and a pipelined architecture that can efficiently perform the DM/invDM without the complex operations of previously proposed methods such as constant composition DM (CCDM). Furthermore, HiDM can operate at a significantly larger post-FEC bit error rate (BER) for the same post-invDM BER performance, which facilitates simulations. These benefits come at the cost of a slightly larger rate loss and required signal-to-noise ratio at a given post-FEC BER.

Index Terms—Bit error rate, block error rate, distribution matching, forward error correction, implementation, modulation, optical fiber communication, probabilistic shaping, reverse concatenation.

I. INTRODUCTION

Multilevel modulation formats have been intensively investigated in coherent optical communications due to the growing traffic demands and requirements for high spectral efficiency. To relax the signal-to-noise ratio (SNR) requirements for such formats, two independent approaches can be employed. The first is *coding*, or forward error correction (FEC), where hard- and soft-decision schemes for fiber-optic communications have demonstrated bit error rates (BER) as low as 10^{-15} [1], [2]. The second is *shaping*, which aims at reducing the average signal power by spherically confining the modulation levels in signal space.

Two shaping approaches can be distinguished; geometric shaping, which uses uniform (equiprobable) modulation levels that are selected to be more or less spherically distributed, and probabilistic shaping (PS), which is based on using low-amplitude constellation points more frequently. Both schemes aim at approximating a Gaussian distribution, which is capacity-achieving for the Gaussian channel. The ultimate SNR improvement for a multidimensional quadrature amplitude modulation (QAM) format relative to the Gaussian channel capacity approaches $\pi e/6$ (1.53 dB) as the number of dimensions approaches to infinity, as shown, e.g., by Forney and Wei [3], who also demonstrated a simple approach to create multidimensional shaped constellations. Calderbank and Ozarow pointed out that an equiprobable (uniform) multidimensional constellation could be viewed as

a lower-dimensional nonequiprobable (nonuniform) signaling scheme [4]. Kschischang and Pasupathy [5] studied nonuniform signaling (probabilistic shaping), and showed that high shaping gains could be realized already for relatively low dimensions and with limited complexity based on Huffman codes. However, the varying bit rate and synchronization problems of such schemes may preclude their usefulness in practical systems. In [6], these drawbacks were proposedly amended by keeping a constant bit-to-symbol rate at the expense of dropping (puncturing) bits.

As coherent optical communication assisted by digital signal processing has been realized [7], multidimensional signaling for optical links has regained interest, and efficient formats were proposed for the inherently four-dimensional optical signals [8]. For the nonlinear optic channel, variants of multidimensional geometric shaping [9]–[12] have been studied, as well as probabilistic shaping [13], [14], based on the scheme proposed in [6].

When combining coding and shaping, there are numerous issues to consider, e.g., the ordering of the schemes and the fact that the presence of one scheme may affect the performance of the other. While these issues were not discussed in the earlier works [3], [5], [8], [9], an outer FEC is often assumed [11], [12], or even necessary [6], [14].

On the other hand, recently Böcherer *et al.* [15] introduced probabilistic amplitude shaping (PAS) based on a *reverse concatenation* architecture, meaning that the FEC coding/decoding is performed inside the shaping algorithm, thus acting on nonuniformly distributed bits. This may realize improved performance and also enable rate adaptation in the shaping scheme rather the FEC, which may provide increased granularity. We note that reverse concatenation was indeed studied much earlier, in [16], and the use of soft-decision FEC was also investigated [17], [18]. Since its emergence, the PAS scheme in the transmitter and its termination in the receiver have been called distribution matching (DM) and distribution dematching (invDM), respectively, and we will use this terminology henceforth.

With normal (nonreverse) concatenation architecture, invDM should be placed before soft-decision FEC decoding. Then soft demapping must convert the multidimensional fine-bit-resolution signals into logarithmic ratios of post-probabilities (*a posteriori* log-likelihood ratios or L-values) [19, Eq. (3.31)] for the decoder, which is prohibitively complex to implement for long codes. On the other hand, reverse concatenation changes the invDM input/output signals to binary sequences. This makes the implementation of invDM much

simpler, and enables the number of dimensions (the code length) to be larger, leading to better performance.

As the DM for reverse concatenation PS, constant composition DM (CCDM) based on arithmetic coding was proposed in [20] and examined for a fiber-optical channel in [21]. These state-of-the-art works show great performance by an almost ideal DM. However, there is room for simplification of these in high-throughput optical fiber communication systems. DM and invDM consume nonnegligible circuit resources, and in practice there will always be implementation penalties relative to the achievable rate that assumes an ideal DM and FEC. In addition, system performance monitoring must be reconsidered when we employ reverse concatenation PS; since the invDM may cause the BER to increase, post-invDM BER should be used instead of post-FEC BER.

In this paper, we propose and analyze in detail a DM scheme, which was briefly introduced in [22]. We compare it with CCDM. We also, for the first time, explain the shaped frame structure, show the result of the DM-to-invDM back-to-back error insertion test, and suggest a method to estimate the post-invDM BER from the post-FEC BER.

This paper is organized as follows: In Secs. II and III, we describe the basic system model and relevant performance metrics. Implementation issues are discussed in Sec. IV, and the proposed DM and framing are discussed in Sec. V. Simulation results comparing our proposed scheme with CCDM are described in Sec. VI. The proposed error-rate estimation is presented in Sec. VII. Summary of the work and future outlook are shown in Sec. VIII.

II. SYSTEM MODEL

Fig. 1 shows the system model and the corresponding performance metrics to be discussed later. We assume the use of pulse amplitude modulation (PAM), which represents a one-dimensional constellation. However, its extension to two-dimensional QAM or optical four-dimensional modulation (two quadratures in two polarizations) is straightforward.

At the transmitter side, the incoming binary sequence is framed into blocks of $\mathbf{A} \in \mathcal{B}^{N_{\text{block}}}$ bits by following, e.g., the modern optical transport network (OTN) standard protocol [23], [24] of $n \times 100\text{G}$ optical transport units (OTUCn), where $\mathcal{B} \in \{0, 1\}$ and N_{block} is the block size of OTUCn, which is $130560n$. A bullet in Fig. 1 indicates a length conversion. In the DM, the binary sequence $\mathbf{A}' \in \mathcal{B}^{N_u}$ is converted to the shaped symbol sequence $\mathbf{D} \in \mathcal{B}^{mN_s}$ including placeholders for FEC parity bits in the following block, where m is the number of bits in the 2^m -PAM symbol, N_u is the number of (uniformly distributed and independent) DM input bits per DM word, and N_s is the DM word length (or the DM output block length). \mathbf{D} corresponds to the PAM symbol sequence $\mathbf{X} \in \mathcal{X}^{N_s}$, where \mathcal{X} denotes a PAM symbol. A systematic binary FEC encoder generates $n_c - k$ (uniformly distributed) parity bits from k payload bits $\mathbf{D}' \in \mathcal{B}^k$, and outputs the FEC codeword $\mathbf{B} \in \mathcal{B}^{n_c}$. The bits $\mathbf{B}' \in \mathcal{B}^m$ are mapped to the PAM symbol $\mathbf{X} \in \mathcal{X}$.

At the receiver side, the received symbol \mathbf{Y} is demapped by bit-metric decoding to *a posteriori* L-values $\mathbf{L}' \in \mathcal{L}^m$

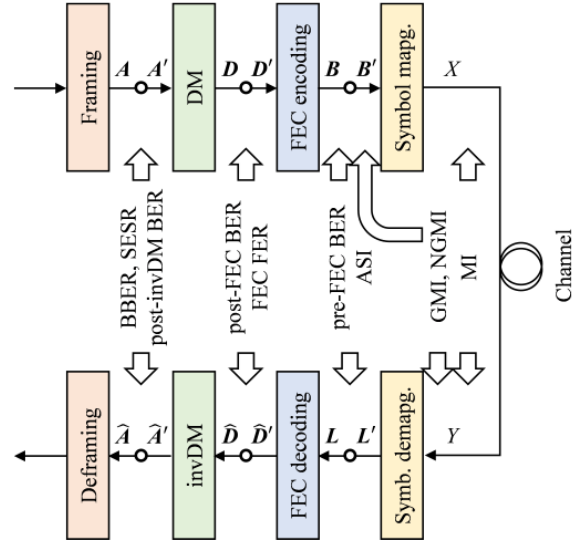


Fig. 1. System model including signal notation and performance metrics.

[19, (3.31)], where \mathcal{L} denotes a continuous or a quantized real number. Based on the L-values $\mathbf{L} \in \mathcal{L}^{n_c}$, FEC decoding recovers the payload bits $\hat{\mathbf{D}}' \in \mathcal{B}^k$. The decoded bit sequence $\hat{\mathbf{D}} \in \mathcal{B}^{mN_s}$ is dematched to $\hat{\mathbf{A}}' \in \mathcal{B}^{N_u}$, and finally $\hat{\mathbf{A}} \in \mathcal{B}^{N_{\text{block}}}$ is deframed.

III. PERFORMANCE METRICS AND PERFORMANCE MONITORING

A. Achievable rates and metrics as post-FEC BER predictor

While the performance requirement for the optical layer has been BER down to 10^{-15} following standards for fiber communications [2], [25], information theory quantifies achievable information rates (AIR) to describe the capacity bounds. The mutual information of the transmitted symbol \mathbf{X} and the received symbol \mathbf{Y} , $I(\mathbf{X}; \mathbf{Y})$, can be a capacity lower bound with nonbinary coding, bit-interleaved coded modulation (BICM) with iterative demapping, or multilevel coded modulation [26]. For BICM without iterative demodulation, an AIR is given by the generalized mutual information (GMI) [19, Sec. 4.3]. The normalized GMI (NGMI, GMI/m) works as a good post-FEC BER predictor for uniform and independent pragmatic signaling [27]. A practical, nonideal FEC has a rate loss, e.g., the required NGMI for a post-FEC BER $< 10^{-15}$ is larger than the FEC code rate R_c [27, Tab. III].

For reverse concatenation PS with bit-metric decoding, an AIR is [15], [28]

$$R_{\text{bmd}}^{\text{ps}} = H(\mathbf{X}) - \sum_{i=1}^m H(B_i | \mathbf{Y}), \quad (1)$$

where $H(\cdot)$ and $H(\cdot | \cdot)$ denote entropy and conditional entropy, resp. $R_{\text{bmd}}^{\text{ps}}$ takes the same value as the GMI calculated for PAS [29], [30]. This can be a common expression for pragmatic BICM and reverse concatenation PS. While $R_{\text{bmd}}^{\text{ps}}$ is the rate with ideal FEC and ideal DM, the information rate with a practical FEC (discussed in the previous paragraph) is defined as

$$R = \frac{N_u}{N_s} \leq H(\mathbf{X}) - (1 - R_c) m, \quad (2)$$

where the symbol entropy $H(X)$ is calculated from the probability mass function (PMF) of the transmitted symbol X , $P_X(x)$, $x \in \mathcal{X}$. Non-ideal DM has a rate loss

$$\Delta = H(X) - (1 - R_c) m - \frac{N_u}{N_s} \geq 0. \quad (3)$$

As post-FEC BER predictors for PS systems using QAM, the NGMI was proposed in [29, (6)]. Using the conditional entropy of B_i given Y and generalizing to arbitrary constellations, it can be shown that the NGMI in [29, (6)] is a special case of

$$\text{NGMI} = 1 - \frac{1}{m} \sum_{i=1}^m H(B_i | Y). \quad (4)$$

The asymmetric information (ASI) [30], [31]

$$\text{ASI} = 1 - h(L_a | |L_a|) \quad (5)$$

was also proposed for the same purpose, where $h(\cdot)$ denotes differential (continuous) entropy. We denote the symmetrized a posteriori L-value, or asymmetric L-value, with $L_a = (-1)^B \cdot L$, where $B \in \mathcal{B}$ is a sample of \mathbf{B} , and $L \in \mathcal{L}$ is a sample of \mathbf{L} corresponding to the sampled bit B . When the channel assumed in the soft-demapping is matched to the true channel, the ASI is equivalent to the NGMI [30]. In practice, however, the soft-demapping circuit operates with a finite bit resolution, which causes a minor performance loss. The GMI or NGMI cannot account for that loss because the received symbol Y is used, but the ASI can because it is based on the L-values just before the FEC decoder. The post-FEC BER can be estimated from the NGMI or the ASI [30]. However, since the performance requirement for reverse concatenation PS is a post-invDM BER of $< 10^{-15}$, one needs to account for a potential BER increase due to the invDM operation. We will discuss this more in Sec. VII.

B. Block performance monitoring

In many modern communication systems, higher-layer protocols apply packet-oriented transmission, where the whole packet is discarded if any bit therein is received in error. BER metrics such as post-FEC BER or post-invDM BER might not be well suited to characterize the performance of such systems. Instead, systems using OTN framing are evaluated based on the background block error rate (BBER) and the severely errored second rate (SESR) [23], [24]. The BBER is equal to the number of erroneous blocks normalized by the total number of transmitted blocks except for the severely errored second (see Sec. II about the block size of OTUCn), and the SESR is the probability of having a fraction of block errors at least the threshold, e.g., 30% or 15%, during one second. As BBER is a more basic performance metric, we will not consider SESR in this paper.

The BBER requirement depends on the link conditions, but a typical values is, e.g., around 10^{-7} . For reverse concatenation PS, a large N_s can cause a long error burst from the residual error after FEC decoding, although a large N_s leads to smaller DM rate loss Δ . As the block performance monitoring is critical for system design, we will simulate and analyze its

behavior in the next section. Note that upper layer packets have smaller or larger sizes compared with the block size of OTUCn, so both the post-invDM BER and the BBER must be considered. In addition, we will consider the FEC frame error rate (FER), which is the probability of an erroneous FEC frame, or codeword, after FEC decoding.

IV. IMPLEMENTATION ISSUES

The state-of-the-art performance of PAS DM is provided by a coding scheme for m -out-of- n codes [32] or CCDM [20]. With this technique, a rate loss Δ of almost zero is possible, provided that the DM word-length is large enough (typically $N_s \sim 10^3 - 10^4$). However, this requires a prohibitively complex hardware implementation. Recently, several attempts have been made to find a better balance between performance and complexity [33]–[38]. In [33], [34], fixed-length to fixed-length conversion was used, which is simple enough to implement, but the performance is limited. In [35], a fixed-length to variable-length conversion scheme with small address sizes look-up tables (LUT) was considered, showing a bounded conversion speed variation. However, this scheme can cause a large error burst after invDM if there is an error before the invDM. A small LUT for a fixed-length to variable-length conversion was combined with a periodical uniformization process in [36] to act as a fixed-length to fixed-length conversion. However, practical implementations of the fixed-length to variable-length conversion requires deeply sequential processing, and a large amount of parallelization (i.e., a large chip area) is required to realize the high throughput. In [37], [38], separate DM is applied to each modulation bit level for efficient implementation, and bit-wise DM like [32], [34], [36] can be combined with it. However, the performance is not as good as the symbol-wise DM in the CCDM.

An FEC coding scheme has another drawback due to the throughput increase from reverse concatenation PS. Consider two cases, nonshaped BICM and reverse concatenation PS, assuming the same client rates, same FEC code rates R_c , and symbol rates. To distinguish the two cases, we introduce m_u and m_s as the number of modulation bits m for the nonshaped and shaped cases, resp. The shaped signal requires m_s/m_u times larger FEC throughput than the nonshaped one, because the bit rate is increased by the DM. Then the FEC circuit size and the power consumption will be increased by the ratio m_s/m_u for the shaped case. Note that there is an FEC code rate restriction of $R_c \geq (m_s - 1)/m_s$ especially in the case of PAS to put the uniformly distributed FEC parity bits to sign-bit positions not to degrade the PMF of $P_{|X|}(|x|)$. In a generalization of the PAS, the parity bits can be placed outside the sign-bit, which relaxes this constraint [34].

V. PROPOSED HIERARCHICAL DM (HiDM)

Here we propose a hierarchical DM (HiDM) for efficient hardware implementation, which was briefly introduced in [22]. The input to the DM in Fig. 1 is the bit sequence $A' \in \mathcal{B}^{N_u}$. Of those bits, N_u^{sb} are converted by the shaping. The number of shaped bit levels is m^{sb} and the number of shaped bits is hence $m^{\text{sb}} N_s$, which is a subset of the DM

TABLE I
THE CONTENTS OF THE LUTS SHOWN IN FIG. 2, INCLUDING EXPECTED SYMBOL POWERS AND PMF.

DM3				DM2				DM1			
input	output	$\mathbb{E}[X ^2]$	PMF	input	output	$\mathbb{E}[X ^2]$	PMF	input	output	$ X $	PMF
000	00 00	21	1/8	00 00	000 000	5	1/8	000 0	0000	1	23/128
001	00 01	41	1/8	00 01	000 001	21	1/8	000 1	0001	3	23/128
010	01 00	41	1/8	00 10	001 000	21	1/8	001 0	0011	5	11/64
011	01 01	61	1/8	00 11	001 001	37	1/8	001 1	0010	7	11/64
100	00 10	63	1/8	01 00	000 010	53	1/16	010 0	0110	9	3/32
101	10 00	63	1/8	01 01	010 000	53	1/16	010 1	0111	11	3/32
110	00 11	83	1/8	01 10	001 010	69	1/16	011 0	0101	13	3/64
111	11 00	83	1/8	01 11	010 001	69	1/16	011 1	0100	15	3/64
				10 00	000 011	101	1/32	100 0	1100	17	1/128
				10 01	011 000	101	1/32	100 1	1101	19	1/128
				10 10	010 010	101	1/32	101 0	1111	21	0
				10 11	001 011	117	1/32	101 1	1110	23	0
				11 00	011 001	117	1/32	110 0	1010	25	0
				11 01	010 011	149	1/32	110 1	1011	27	0
				11 10	011 010	149	1/32	111 0	1001	29	0
				11 11	000 100	165	1/32	111 1	1000	31	0

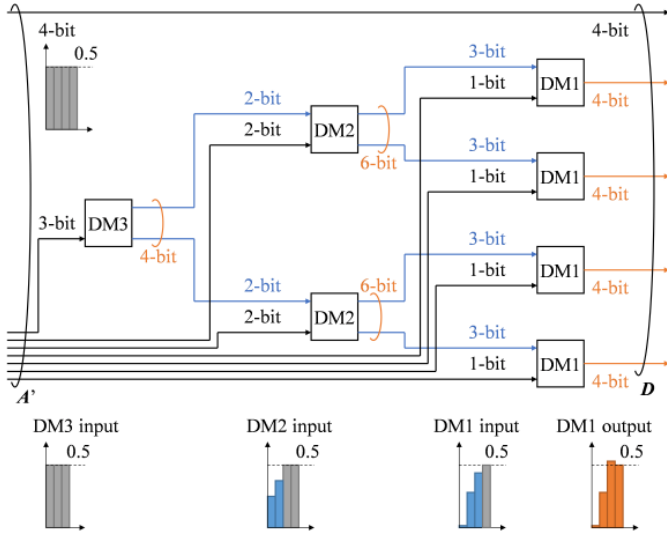


Fig. 2. Example of the proposed hierarchical DM (HiDM), where 15 uniform input bits A' are converted into 20 output bits D (4 uniform and 16 shaped bits). Bar charts illustrate bit probabilities.

output bits $D \in \mathcal{B}^{mN_s}$. The parameters m , m^{sb} , N_u , N_u^{sb} , N_s have a relation with FEC code rate R_c as

$$\frac{N_u - N_u^{sb}}{N_s} = R_c m - m^{sb}. \quad (6)$$

Next we will explain how N_u^{sb} uniform input bits can be converted into $m^{sb}N_s$ nonuniform (probabilistically shaped) bits.

A. Operation principle

A small example of the proposed HiDM for generating a sequence of four PS-32-PAM symbols is shown in Fig. 2, where $m = 5$, the shaped bit levels $\hat{i}_{sb} = (2, 3, 4, 5)$, $m^{sb} = |\hat{i}_{sb}| = 4$, $N_u^{sb} = 11$, and $N_s = 4$ (i.e., four PAM symbols). For simplicity, we assume here an FEC code rate of $R_c = 1$. Hence, the DM has 15 uniform input bits and 20

output bits. Four of the input bits remain untouched by the DM, while 11 input bits are converted into 16 shaped bits. The DM consists of three small DMs, called DM1, DM2, and DM3, hierarchically organized in a tree-like structure with three layers. Each layer comprise one or more DMs, which are the same within each layer. The LUT contents including the expected one-dimensional power $\mathbb{E}[|X|^2]$ and probabilities of each small-DM word, PMF, are shown in Tab. I. The expected power is derived from the expected powers in the lower layer, e.g., $\mathbb{E}[|X|^2]$ for output bits "000 001" (the second small DM word) in DM2 is the average power for a bit input to DM1 "000d" (i.e., $(1^2 + 3^2)/2 = 5$) and "001d" (i.e., $(5^2 + 7^2)/2 = 37$), where "d" denotes don't care of "0" or "1". Then $\mathbb{E}[|X|^2]$ of $(5 + 37)/2 = 21$ is obtained as shown in the second word in DM2. Each list is sorted from lower to higher powers, and lower power ones are chosen frequently by the constraint from the upper layer. At first, three uniformly distributed information bits are input to DM3 and converted into four output bits, which will act as constraint bits in the connected lower-layer DMs. The four constraint bits are separated into two lines of two constraint bits each having expected mark ratios of 0.25 and 0.375, which together with two uniformly distributed information bits are fed into each DM2. The constraint bits are chosen so that the expected power becomes small. This corresponds that each list in Tab. I is sorted by the expected power. DM2 converts four input bits into six output bits, which are again separated into two lines and treated as constraints bits in the next layer. Complementing each set of three constraint bits having expected mark ratios of 0.016, 0.281, and 0.438 with one uniformly distributed information bit, each DM1 generates four output bits having expected mark ratios of 0.016, 0.300, 0.531, and 0.5. Note that the output bits from DM3, DM2, or DM1 are dependent. These output bits from DM1 will determine the absolute amplitudes $|X|$ of the symbol sequence X . In this example, the probability of $|X|$ becomes 0.445, 0.445, 0.437, 0.437, 0.320, 0.320, 0.207, 0.207, 0.055, 0.055, 0, 0, 0, 0, 0, 0 for $|X| = 1, 3, \dots, 31$. Note that the output bits from each DM

are dependent. The information rate of the PAM symbol is $15/20 \times 5 = 3.75$, and the entropy is 3.93, then the rate loss Δ becomes 0.177 in one dimension. When the five output bits are mapped to a Gray-coded 32-PAM symbol, the expected power per one-dimensional symbol is 57. Then the constellation gain [5] will be 0.22 dB.

The proposed hierarchical architecture constrain the output bits from the connected lower-layer DMs. The upper-layer DM is designed so that its output roughly matches the desired bit distribution by constraining the subset of the output bits at the lower layers, and the lower-layer DMs gradually refine the distribution for better agreement with the target. Additional flexibility and finer granularity can be obtained by increasing the number of layers, the number of DMs connected between layers, the number of input information bits to each layer's DM, and the number of constraint bits in each layer, which gives better control of the output signal distribution and more significant performance improvements. Each DM function is one-to-one correspondence, so it is reversible at the invDM.

B. Complexity

The complexity of the required circuitry is dominated by the number of stored bits in the LUTs, which determines the area in the hardware implementation. The number of stored bits depends on the number of words (addresses), the number of output bits, and the number of LUTs. In the example in Fig. 2, the number of stored bits are $2^3 \times 4 \times 1 = 32$ for DM3, $2^4 \times 6 \times 2 = 192$ for DM2, and $2^4 \times 4 \times 4 = 256$ for DM1, thus in total 480. The corresponding LUTs on the invDM side have $2^4 \times 3 \times 1 = 48$ stored bits in layer 3, $2^6 \times 4 \times 2 = 512$ in layer 2, and $2^4 \times 4 \times 4 = 256$ in layer 1, which totals 816 stored bits. If we instead would use a single LUT, i.e., 11-bit input and 16-bit output on the DM side and conversely on the invDM side, the number of stored bits would be $2^{11} \times 16 = 32768$ and $2^{16} \times 11 = 720896$, resp. Thus, HiDM saves circuit resources by a factor of 68 and 883 in the DM and invDM, resp., already in this small-scale example.

DM schemes with word length $N_s \approx 100$ or 1000 can be realized by LUTs with reasonable sizes. The DM does thus not require complex operations such as integer additions or multiplications. The conversion process is purely fixed-length input and fixed-length output (there is no variable length part). Either bit-wise [37] or symbol-wise [20] DMs are possible, and arbitrary output distributions can be approximated with high granularity. This is not constant composition DM, but its PMF will converge to the target for sufficiently many DM words. This DM achieves a high throughput because the architecture consists of a fully parallelized input/output configuration, as well as a bit-scramble selector and a permutation mapper [34]. The hierarchical operation is fully pipelined, so a small number of instances is enough.

In contrast, a coding scheme for m -out-of- n codes such as the CCDM requires high-precision integer multiplications, which limits the throughput, and a large number of instances (at least $\sim N_s$) would be required. Then the equivalent DM word-length is in the order of N_s^2 or more, as will be further discussed in the next section.

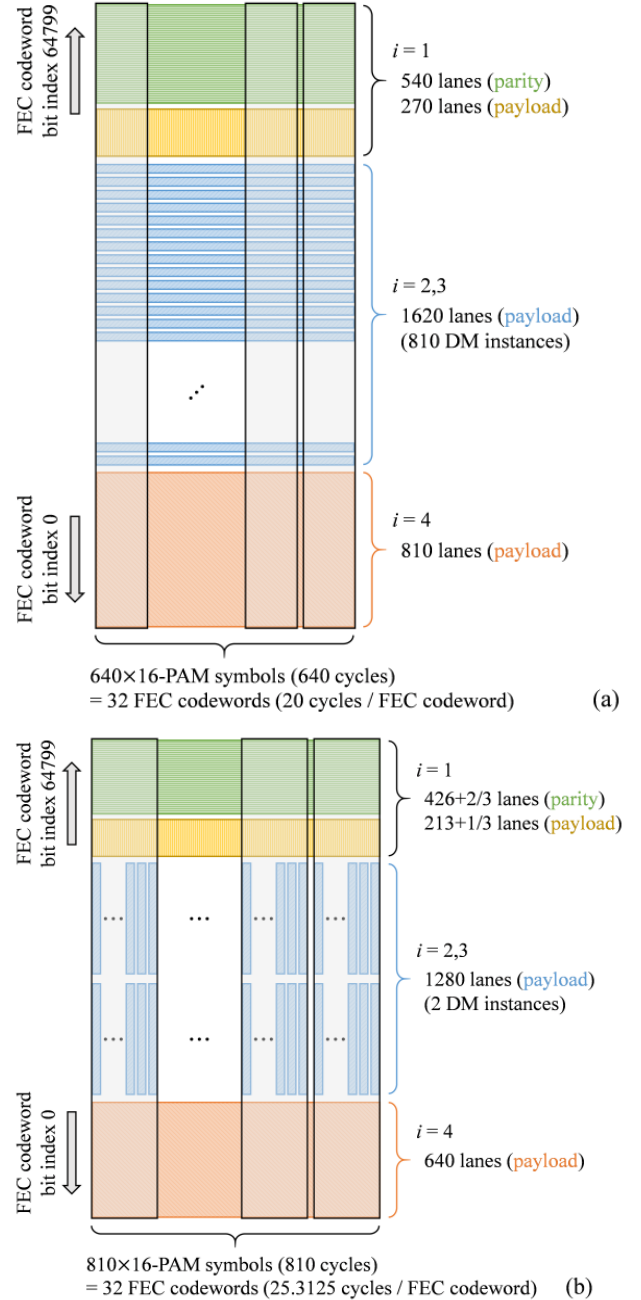


Fig. 3. Line-side frame structure with (a) CCDM or with (b) HiDM.

C. Frame structure

An example of a line-side frame structure with the CCDM (a) and the proposed HiDM (b) are shown in Fig. 3. The FEC is assumed to be a DVB-S2 low-density parity-check code [39] with codeword length $n_c = 64800$ and code rate $R_c = 5/6$. The modulation format is Gray-coded 16-PAM. The most significant ($i = 1$, sign-bit) and the least significant ($i = 4$) bit-levels for the 16-PAM symbols are not shaped to simplify the implementation. Thus, $m^{sb} = 2$ and the shaped bit levels $i_{sb} = \{2, 3\}$. The number of input bits N_u^{sb} is 1014 or 507, the number of output symbols N_s is 640 or 320, and the number of output bits $m^{sb} N_s$ is 1280 or 640 for CCDM or HiDM, resp., in this example. The HiDM is designed using seven layers. In

the bottom layer, there are 64 small DMs (DM1), each having 10 output bits. Thus, the total number output bits from the proposed DM is 640, which equals $m^{\text{sb}}N_s$.

The information rate ($R - \Delta$) is 5.83 bit/channel use, which is equivalent to 128-QAM with $R_c = 5/6$. The equivalent word-length for CCDDM and HiDM are 518400 ($> N_s^2$) and 320, resp. While 810 DM words are equally mapped to 32 FEC codewords in parallel for the CCDDM, 50 or 51 DM words are included in an FEC codeword sequentially for the HiDM. The bit indices 0–53999 of the FEC codeword correspond to the payload bits and indices 54000–64799 of the parity bits. The less significant bits are placed at lower bit-indices of the FEC codeword to balance the pre-FEC performance and the FEC decoding capability.

VI. SIMULATIONS

To evaluate the post-FEC and post-invDM performance with reverse concatenation PS, we conducted numerical simulations of PS-256-QAM transmission over the Gaussian channel. The examined the same combinations of FEC and PS as in Sec. V, i.e., the DVB-S2 low-density parity-check code with $R_c = 5/6$. The number of decoding iterations was 20 and more than 1600 FEC codewords were examined per simulation. The soft-demapping input and output interfaces were quantized with 7 and 4 bits, resp., which gives less than 0.1 dB SNR penalty. Two DM schemes were implemented, HiDM and CCDDM, and for comparison we also simulated nonshaped BICM 128-QAM, whose most significant bit ($i = 1$) and parts of the second significant bit ($i = 2$) were occupied by the FEC parity bits, for the same information rate.

Fig. 4 shows the simulation results in terms of post-FEC BER, post-invDM BER, FER, and BBER as a function of the SNR. Here we assume the use of OTUC1 framing, so the block size is 130560 bits. The post-FEC BER at low BERs is similar among the bit levels, due to the bit level mapping in the FEC codeword space [15]. CCDDM shows 0.13 dB lower required SNR than HiDM at a post-FEC BER of 10^{-6} , and 128-QAM BICM performed further 0.8 dB worse than HiDM. The error rate increase by the invDM for the reverse concatenation PS is characterized by the post-invDM BER $\mathcal{E}_{\text{post-invDM}}$ to post-FEC BER $\mathcal{E}_{\text{post-FEC}}$ ratio,

$$r_{\mathcal{E}1} = \frac{\mathcal{E}_{\text{post-invDM}}}{\mathcal{E}_{\text{post-FEC}}}, \quad (7)$$

which are 200 and 5.5 for CCDDM and HiDM, resp., at around $\mathcal{E}_{\text{post-FEC}} = 10^{-6}$. This relation is expected to be valid also at lower error rates, according to the analysis in the next section.

To quantify the amount of burst errors after the invDM, the ratio of BBER $\mathcal{E}_{\text{block}}$ to post-invDM BER $\mathcal{E}_{\text{post-invDM}}$,

$$r_{\mathcal{E}2} = \begin{cases} \mathcal{E}_{\text{block}}/\mathcal{E}_{\text{post-invDM}} & (\text{CCDDM, HiDM}) \\ \mathcal{E}_{\text{block}}/\mathcal{E}_{\text{post-FEC}} & (\text{BICM}) \end{cases}, \quad (8)$$

is useful, which is found to be 500, 11000, and 20000 for CCDDM-based PS-256-QAM, HiDM-based PS-256-QAM, and BICM 128-QAM, respectively, as shown in Fig. 4. If $r_{\mathcal{E}2}$ is smaller, the erroneous frame has a larger number of errors, so the error bursts are more severe. The error burstiness of HiDM-based PS-256-QAM is $11000/500 = 22$ times lower than with

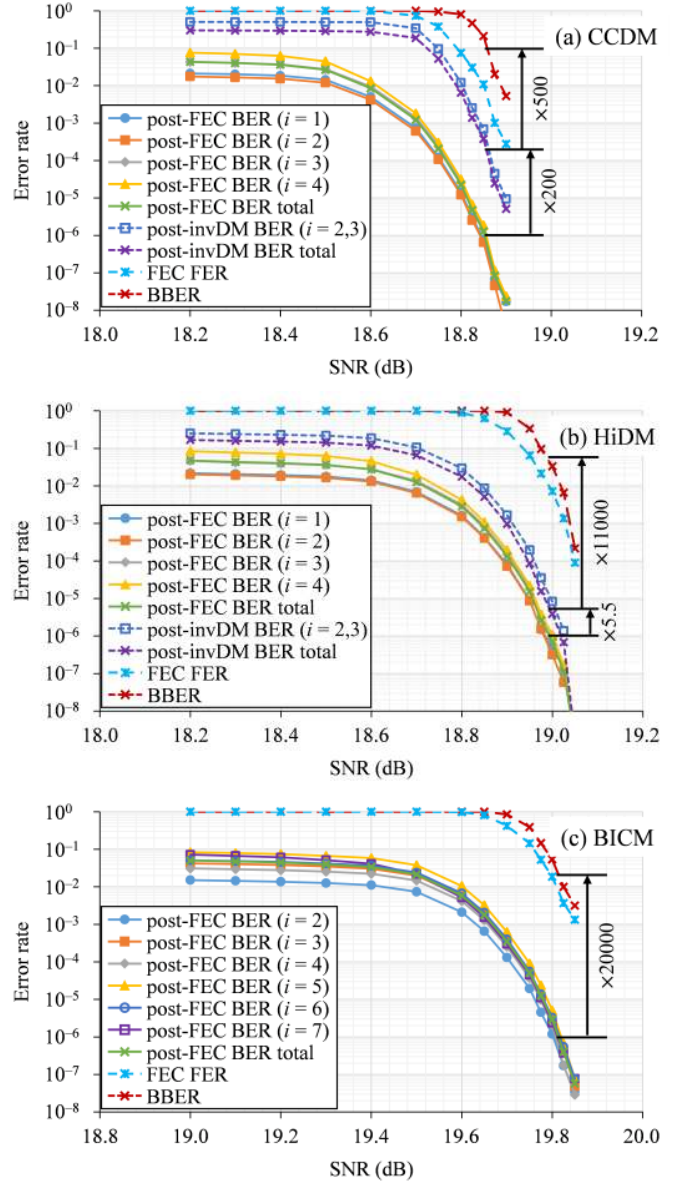


Fig. 4. Simulation results of (a) CCDDM-based PS-256-QAM, (b) HiDM-based PS-256-QAM, and (c) BICM-based 128-QAM.

CCDDM. It means that the HiDM can be concatenated with an outer hard-decision FEC if needed because of the significant reduction of the burstiness of the residual errors.

VII. POST-INVDM PERFORMANCE ESTIMATION AT LOW ERROR RATES

We try to estimate the post-invDM BER from the post-FEC BER by inserting random errors into each DM word before the invDM operation. Fig. 5 shows the simulation configuration for the DM to invDM back-to-back error insertion test. As before, the shaped bit levels are $i_{\text{sb}} = \{2, 3\}$ and $m^{\text{sb}} = 2$. The number of information bits $N_u^{\text{sb}} = 1014$ and 507 for CCDDM and HiDM, resp. The information bits were fed to the DM, $m^{\text{sb}}N_s = 2N_s$ shaped bits were generated, errors were inserted into the shaped bits, and the invDM recovered the shaped information.

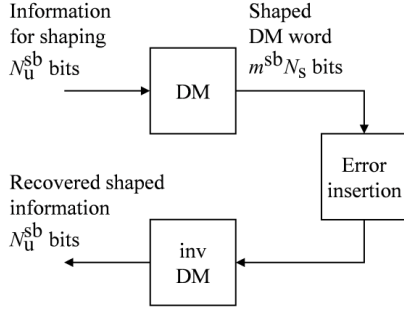


Fig. 5. Simulation setup for DM to invDM back-to-back error insertion test.

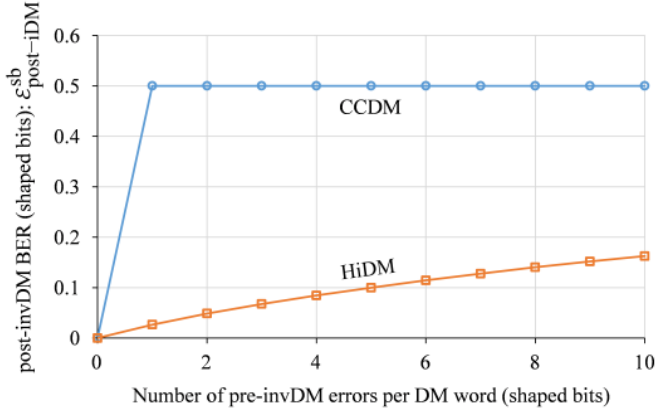


Fig. 6. Simulated post-invDM BER under single error per a DM word at the input of invDM for PS-256-QAM.

Fig. 6 shows the simulated post-invDM BER $\mathcal{E}_{\text{post-iDM}}^{\text{sb}}$ as a function of the number of erroneous bits per DM word, both computed for the shaped bits only. The expected value of $\mathcal{E}_{\text{post-iDM}}^{\text{sb}}$ for CCDM is 0.5 for any number of errors, whereas for HiDM it increases from 0.027 for a single error to 0.16 for 10 errors. The expected number of errors after post-invDM α is 507 for CCDM and 13.4 for HiDM with a single bit error.

The ratio $r_{\mathcal{E}_1}$ of 200 or 5.5 in the previous section corresponds to the expected error count under the single-error input assumption. Although the FEC decoder can output an error burst, at least the bit-level dependence is weak according to the simulation results in Fig. 4. Under the single-error input condition, the post-invDM BERs for the shaped bits and the total bits, $\mathcal{E}_{\text{post-iDM}}^{\text{sb}}$ and $\mathcal{E}_{\text{post-iDM}}^{\text{total}}$, are bounded as

$$\mathcal{E}_{\text{post-iDM}}^{\text{sb}} \leq \min \left\{ \frac{\alpha \cdot m^{\text{sb}} N_s}{N_u^{\text{sb}}} \mathcal{E}_{\text{post-FEC}}, \frac{1}{2} \right\}, \quad (9)$$

$$\mathcal{E}_{\text{post-iDM}}^{\text{total}} \leq \gamma_{\text{in}} \mathcal{E}_{\text{post-iDM}}^{\text{sb}} + (1 - \gamma_{\text{in}}) \mathcal{E}_{\text{post-FEC}}. \quad (10)$$

The fractions of shaped DM input and output bits (i.e., the fractions of \mathbf{A}' and \mathbf{D} that are shaped in the DM) are, resp.,

$$\gamma_{\text{in}} = \frac{N_u^{\text{sb}}}{N_u}, \quad (11)$$

$$\gamma_{\text{out}} = \frac{m^{\text{sb}}}{R_c m}. \quad (12)$$

The BBER can be bounded as

$$\mathcal{E}_{\text{block}} \leq \min \left\{ \frac{N_{\text{block}} (\gamma_{\text{out}} \beta + 1 - \gamma_{\text{out}})}{k \cdot N_u / (m N_s R_c)} \mathcal{E}_{\text{FEC-fr}}, 1 \right\}, \quad (13)$$

TABLE II
SINGLE-ERROR PARAMETERS

	CCDM	HiDM	BICM
α	507	13.4	—
β	32	≤ 2	1
γ_{in}	0.543	0.543	0
γ_{out}	0.6	0.6	0

	$\mathcal{E}_{\text{post-iDM}}^{\text{total}}$		$\mathcal{E}_{\text{block}}$	
	Sim.	Est.	Sim.	Est.
CCDM	○	—	●	⋯
HiDM	□	- - -	■	- - -
BICM	△	- - -	▲	- - -

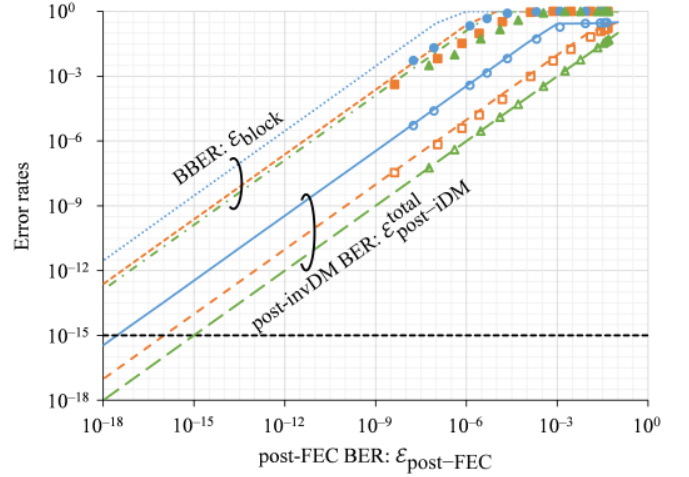


Fig. 7. post-invDM BER from simulation or estimation under the assumption of the single-error input to the invDM per a DM word.

where the FEC FER $\mathcal{E}_{\text{FEC-fr}}$ is also bounded as

$$\mathcal{E}_{\text{FEC-fr}} \leq \min \{ k \cdot \mathcal{E}_{\text{post-FEC}}, 1 \}. \quad (14)$$

The parameters α and β , which denote the number of output error bits of the invDM with a single-error input, and the number of OTUC1 block errors with a single FEC codeword error, resp., are shown in Tab. II, along with γ_{out} and γ_{in} . In the simulations, the number of information bits for the FEC is $k = 54000$. If the expected number of errors in an erroneous FEC codeword is larger than 1 due to the bursty nature of FEC decoders, $\mathcal{E}_{\text{FEC-fr}}$ becomes closer to $\mathcal{E}_{\text{post-FEC}}$. The quantity $N_u / (m N_s R_c)$ in (13) is 0.875 for CCDM/HiDM-based PS-256-QAM and 1 for BICM-based 128-QAM.

The ratio $r_{\mathcal{E}_1}$ can be calculated based on (9) and (10), which gives $r_{\mathcal{E}_1}$ is 348 and 9.7 for CCDM and HiDM, respectively. These theoretic results are of the same order as the simulation results in the previous section. This single-error scenario gives the largest $r_{\mathcal{E}_1}$ (the post-invDM BER would be worse than the case with burst errors).

In Fig. 7, we estimated the post-invDM BER and BBER as a function of the post-FEC BER at low error rates using the bounds (10) and (13). The post-invDM BER $\mathcal{E}_{\text{post-iDM}}^{\text{total}}$ estimates agree well with the simulation results. To achieve a post-invDM BER of 10^{-15} , a post-FEC BER of $3 \cdot 10^{-18}$

(for CCDM) or 10^{-16} (for HiDM) is required. We can thus conclude that the FEC design and evaluation becomes more difficult with reverse concatenation PS than with BICM, due to the requirement of such low post-FEC BERs. If the code would have an error floor just below a post-FEC BER of 10^{-15} , the required SNR for a post-invDM BER of 10^{-15} would be significantly larger. Also, simulations to evaluate a post-FEC BER of $3 \cdot 10^{-18}$ to ensure that there is no error floor are very challenging (to transmit 10^{18} bits at 100 Gbit/s takes 10^7 s, or 3.8 months.) HiDM requires an order of magnitude higher error rate than CCDM, so the gap between BICM and reverse concatenation PS is greatly reduced. As for the BBER $\mathcal{E}_{\text{block}}$, the estimation and the simulation approach each other in the low post-FEC BER regime, where the single-error assumption would work well. The bounded BBER as a function of the post-FEC BER for HiDM is almost the same as for BICM-based 128-QAM. The BBER bound for HiDM is 16 times lower than for CCDM in the case of the same post-FEC BER, because the HiDM places the DM word on the local area due to the high throughput feature compared with the CCDM, as shown in Fig. 3.

VIII. SUMMARY AND OUTLOOK

We proposed HiDM for low-complexity implementation of reverse-concatenation PS, and evaluated its end-to-end performance for high-throughput fiber-optic communications. As the post-invDM BER and BBER performance depends on the FEC decoding, invDM processing, and cross-layout of the FEC codewords and the DM words, we demonstrated frame structure examples considering the combined FEC and PS. By a back-to-back error insertion test and a single-error assumption, very low post-invDM error rates can be estimated from the post-FEC BER, which allows relaxed requirements for post-FEC BER if HiDM is used instead of CCDM. The combination of known post-FEC BER prediction techniques using NGMI or ASI with the proposed post-invDM error rate estimation from post-FEC BER would be interesting for further studies. Other future research directions include a careful design of DM/invDM algorithms considering the implementation combined with FEC to reach the desired BER and BBER performance targets.

ACKNOWLEDGMENTS

We thank Alex Alvarado of Eindhoven University of Technology and Koji Igarashi of Osaka University for fruitful discussions about performance metrics and reverse concatenation.

REFERENCES

- [1] F. Chang, K. Onohara, and T. Mizuochi, "Forward error correction for 100 G transport networks," *IEEE Commun. Mag.*, vol. 48, no. 3, pp. S48–S55, Mar. 2010.
- [2] E. Agrell and M. Secondini, "Information-theoretic tools for optical communications engineers," to appear in *Proc. IEEE Phot. Conf. (IPC)*, Reston, VA, Sep.–Oct. 2018.
- [3] G. D. Forney, Jr. and L.-F. Wei, "Multidimensional constellations—Part I: introduction, figure of merit, and generalized cross constellation," *IEEE J. Selected Areas Commun.*, vol. 7, no. 6, pp. 877–892, Aug. 1989.
- [4] A. R. Calderbank and L. H. Ozarow, "Nonequiprobable signaling on the Gaussian channel," *IEEE Trans. Inf. Theory*, vol. 36, no. 4, pp. 726–740, July 1990.
- [5] F. R. Kschischang and S. Pasupathy, "Optimal nonuniform signaling for Gaussian channels," *IEEE Trans. Inf. Theory*, vol. 39, no. 3, pp. 913–929, May 1993.
- [6] D. Raphaeli and A. Gurevitz, "Constellation shaping for pragmatic turbo-coded modulation with high spectral efficiency," *IEEE Trans. Commun.*, vol. 52, no. 3, pp. 341–345, Mar. 2004.
- [7] K. Roberts, M. O'Sullivan, K.-T. Wu, H. Sun, A. Awadalla, D. J. Krause, and C. Laperle, "Performance of dual-polarization QPSK for optical transport systems," *J. Lightw. Technol.*, vol. 27, no. 16, pp. 3546–3559, Aug. 2009.
- [8] E. Agrell and M. Karlsson, "Power-efficient modulation formats in coherent transmission systems," *J. Lightw. Technol.*, vol. 27, no. 22, pp. 5115–5126, Nov. 2009.
- [9] R. Dar, M. Feder, A. Mecozzi, and M. Shtaif, "On the shaping gain in the nonlinear fiber-optic channel," in *Proc. IEEE Int. Symp. Inf. Theory*, pp. 2794–2798, July 2014.
- [10] D. S. Millar, T. Koike-Akino, S. Ö. Arık, K. Kojima, K. Parsons, T. Yoshida, and T. Sugihara, "High-dimensional modulation for coherent optical communications systems," *Opt. Exp.*, vol. 22, no. 7, pp. 8798–8812, Apr. 2014.
- [11] A. D. Shiner, M. Reimer, A. Borowiec, S. O. Gharan, J. Gaudette, P. Mehta, D. Charlton, K. Roberts, and M. O'Sullivan, "Demonstration of an 8-dimensional modulation format with reduced inter-channel nonlinearities in a polarization multiplexed coherent system," *Opt. Exp.*, vol. 22, no. 17, pp. 20366–20374, Aug. 2014.
- [12] K. Kojima, T. Yoshida, T. Koike-Akino, D. S. Millar, K. Parsons, M. Pajovic, and V. Arlunno, "Nonlinearity-tolerant four-dimensional 2A8PSK family for 5–7 bits/symbol spectral efficiency," *J. Lightw. Technol.*, vol. 35, no. 8, pp. 1383–1391, Apr. 2017.
- [13] L. Beygi, E. Agrell, J. M. Kahn, and M. Karlsson, "Rate-adaptive coded modulation for fiber-optic communications," *J. Lightw. Technol.*, vol. 32, no. 2, pp. 333–343, Jan. 2014.
- [14] M. P. Yankov, F. D. Ros, E. P. da Silva, S. Forchhammer, K. J. Larsen, L. K. Oxenløwe, M. Galili, and D. Zibar, "Constellation shaping for WDM systems using 256QAM/1024QAM with probabilistic optimization," *J. Lightw. Technol.*, vol. 34, no. 22, pp. 5146–5156, Nov. 2016.
- [15] G. Böcherer, F. Steiner, and P. Schulte, "Bandwidth efficient and rate-matched low-density parity-check coded modulation," *IEEE Trans. Commun.*, vol. 63, no. 12, pp. 4651–4665, Dec. 2015.
- [16] W. G. Bliss, "Circuitry for performing error correction calculations on baseband encoded data to eliminate error propagation," *IBM Techn. Discl. Bul.*, vol. 23, pp. 4633–4634, 1981.
- [17] J. L. Fan and J. M. Cioffi, "Constrained coding techniques for soft iterative decoders," in *Proc. Global Telecommunications Conference (GLOBECOM)*, Rio de Janeiro, Brazil, Dec. 1999, vol. 1(B), pp. 723–727.
- [18] I. B. Djordjevic and B. V. Vasic, "Constrained coding techniques for the suppression of intrachannel nonlinear effects in high-speed optical transmission," *J. Lightw. Technol.*, vol. 24, no. 1, pp. 411–419, Jan. 2006.
- [19] L. Szczecinski and A. Alvarado, *Bit-Interleaved Coded Modulation: Fundamentals, Analysis, and Design*. New York, NY, USA: Wiley, 2015.
- [20] P. Schulte and G. Böcherer, "Constant composition distribution matching," *IEEE Trans. Inf. Theory*, vol. 62, no. 1, pp. 430–434, Jan. 2016.
- [21] F. Buchali, F. Steiner, G. Böcherer, L. Schmalen, P. Schulte, and W. Idler, "Rate adaptation and reach increase by probabilistically shaped 64-QAM: an experimental demonstration," *J. Lightw. Technol.*, vol. 34, no. 7, pp. 1599–1609, Apr. 2016.
- [22] T. Yoshida, M. Karlsson, and E. Agrell, "Technologies toward implementation of probabilistic constellation shaping," in *Proc. Eur. Conf. on Opt. Comm. (ECOC)*, Roma, Italy, Sep. 2018, p. Th.1.H.1.
- [23] ITU-T, "Interfaces for the optical transport network," 2016. [Online]. Available: www.itu.int/rec/T-REC-G.709
- [24] ITU-T, "Error performance parameters and objectives for multioperator international paths within optical transport networks," 2011. [Online]. Available: www.itu.int/rec/T-REC-G.8201
- [25] ITU-T, "Forward error correction for high bit-rate DWDM submarine systems," 2004. [Online]. Available: www.itu.int/rec/T-REC-G.975.1
- [26] L. Schmalen, A. Alvarado, R. Rios-Müller, "Performance prediction of nonbinary forward error correction in optical transmission experiments," *J. Lightw. Technol.*, vol. 35, no. 4, pp. 1015–1027, Feb. 2017.
- [27] A. Alvarado, E. Agrell, D. Lavery, R. Maher, and P. Bayvel, "Replacing the soft FEC limit paradigm in the design of optical communication systems," *J. Lightw. Technol.*, vol. 33, no. 20, pp. 4338–4352, Oct. 2015.
- [28] G. Böcherer, "Achievable rates for probabilistic shaping," [Online]. Available: www.arxiv.org/pdf/1707.01134v4

- [29] J. Cho, L. Schmalen, and P. J. Winzer, "Normalized generalized mutual information as a forward error correction threshold for probabilistically shaped QAM," in *Proc. Eur. Conf. Opt. Commun. (ECOC)*, Göteborg, Sweden, Sep. 2017, p. M.2.D.2.
- [30] T. Yoshida, M. Karlsson, and E. Agrell, "Performance metrics for systems with soft-decision FEC and probabilistic shaping," *Photon. Technol. Lett.*, vol. 29, no. 23, pp. 2111–2114, Dec. 2017.
- [31] T. Yoshida, M. Karlsson, and E. Agrell, "Post-FEC BER prediction accuracy for probabilistically shaped signaling in fiber-optic communications," in *Proc. Eur. Conf. on Opt. Comm. (ECOC)*, Göteborg, Sweden, Sep. 2017, p. Mo.2.D.3.
- [32] T. V. Ramabadran, "A coding scheme for m -out-of- n codes," *IEEE Trans. Commun.*, vol. 38, no. 8, pp. 1156–1163, Aug. 1990.
- [33] J. Cho, S. Chandrasekhar, R. Dar, and P. J. Winzer, "Low-complexity shaping for enhanced nonlinearity tolerance," in *Proc. Eur. Conf. on Opt. Comm. (ECOC)*, Düsseldorf, Germany, Sep. 2016, p. W1C.2.
- [34] T. Yoshida, M. Karlsson, and E. Agrell, "Short-block-length shaping by simple mark ratio controllers for granular and wide-range spectral efficiencies," in *Proc. Eur. Conf. on Opt. Comm. (ECOC)*, Göteborg, Sweden, Sep. 2017, p. Tu.2.D.2.
- [35] G. Böcherer, F. Steiner, and P. Schulte, "Fast probabilistic shaping implementation for long-haul fiber-optic communication systems," in *Proc. Eur. Conf. on Opt. Comm. (ECOC)*, Göteborg, Sweden, Sep. 2017, p. Tu.2.D.3.
- [36] T. Yoshida, M. Karlsson, and E. Agrell, "Low-complexity variable-length output distribution matching with periodical distribution uniformization," in *Proc. Opt. Fib. Commun. Conf. (OFC)*, San Diego, CA, USA, Mar. 2018, p. M.4.E.2.
- [37] M. Pikus and W. Xu, "Bit-level probabilistically shaped coded modulation," *IEEE Commun. Lett.*, vol. 21, no. 9, pp. 1929–1932, Sep. 2017.
- [38] G. Böcherer, F. Steiner, and P. Schulte, "High throughput probabilistic shaping with product distribution matching," [Online]. Available: www.arxiv.org/pdf/1702.07510v4
- [39] European Telecommunications Standards Institute, "Second generation framing structure, channel coding and modulation systems for broadcasting, interactive services, news gathering and other broadband satellite applications; Part 1 (DVB-S2)," ETSI Standard EN 302 307-1 V1.4.1, Nov. 2014. [Online]. Available: www.dvb.org/standards